# Identification of deformed intruder states in semi-magic $^{70}$Ni

C. J. Chiara,[1, 2, *] D. Weisshaar,[3] R. V. F. Janssens,[2] Y. Tsunoda,[4] T. Otsuka,[4, 5, 3] J. L. Harker,[1, 2]
W. B. Walters,[1] F. Recchia,[3, 6] M. Albers,[2, †] M. Alcorta,[2, ‡] V. M. Bader,[3, 7, §] T. Baugher,[3, 7, ¶] D. Bazin,[3, 7]
J. S. Berryman,[3] P. F. Bertone,[2, **] C. M. Campbell,[8] M. P. Carpenter,[2] J. Chen,[9] H. L. Crawford,[8]
H. M. David,[2, 10] D. T. Doherty,[2, 10, ††] A. Gade,[3, 7] C. R. Hoffman,[2] M. Honma,[11] F. G. Kondev,[9]
A. Korichi,[12, 2] C. Langer,[3, 13] N. Larson,[3, 14] T. Lauritsen,[2] S. N. Liddick,[3, 14] E. Lunderberg,[3, 7]
A. O. Macchiavelli,[8] S. Noji,[3] C. Prokop,[3, 14] A. M. Rogers,[2, ‡‡] D. Seweryniak,[2] N. Shimizu,[5]
S. R. Stroberg,[3, 7, ‡] S. Suchyta,[3, 14, §§] Y. Utsuno,[15] S. J. Williams,[3] K. Wimmer,[3, 16, ¶¶] and S. Zhu[2]

$^1$*Department of Chemistry and Biochemistry, University of Maryland, College Park, Maryland 20742, USA*
$^2$*Physics Division, Argonne National Laboratory, Argonne, Illinois 60439, USA*
$^3$*National Superconducting Cyclotron Laboratory, Michigan State University, East Lansing, Michigan 48824, USA*
$^4$*Department of Physics, University of Tokyo, Hongo, Bunkyo-ku, Tokyo 113-0033, Japan*
$^5$*Center for Nuclear Study, University of Tokyo, Hongo, Bunkyo-ku, Tokyo 113-0033, Japan*
$^6$*Dipartimento di Fisica e Astronomia, Università degli Studi di Padova, I-35131 Padova, Italy*
$^7$*Department of Physics and Astronomy, Michigan State University, East Lansing, Michigan 48824, USA*
$^8$*Nuclear Science Division, Lawrence Berkeley National Laboratory, Berkeley, California 94720, USA*
$^9$*Nuclear Engineering Division, Argonne National Laboratory, Argonne, Illinois 60439, USA*
$^{10}$*School of Physics and Astronomy, University of Edinburgh, Edinburgh, EH9 3JZ, UK*
$^{11}$*Center for Mathematical Sciences, University of Aizu, Aizu-Wakamatsu, Fukushima 965-8580, Japan*
$^{12}$*CSNSM-IN2P3/CNRS, F-91405 Orsay Campus, France*
$^{13}$*Joint Institute for Nuclear Astrophysics, Michigan State University, East Lansing, Michigan 48824, USA*
$^{14}$*Department of Chemistry, Michigan State University, East Lansing, Michigan 48824, USA*
$^{15}$*Advanced Science Research Center, Japan Atomic Energy Agency, Tokai, Ibaraki 319-1195, Japan*
$^{16}$*Department of Physics, Central Michigan University, Mt. Pleasant, Michigan 48859, USA*
(Dated: March 19, 2015)

The structure of semi-magic $^{70}_{28}$Ni$_{42}$ was investigated following complementary multinucleon-transfer and secondary fragmentation reactions. Changes to the higher-spin, presumed negative-parity states based on observed $\gamma$-ray coincidence relationships result in better agreement with shell-model calculations using effective interactions in the neutron $f_{5/2}pg_{9/2}$ model space. The second $2^+$ and $(4^+)$ states, however, can only be successfully described when proton excitations across the $Z = 28$ shell gap are included. Monte-Carlo shell-model calculations suggest that the latter two states are part of a prolate-deformed intruder sequence, establishing an instance of shape coexistence at low excitation energies similar to that observed recently in neighboring $^{68}$Ni.

PACS numbers: 23.20.Lv, 21.10.Hw, 21.60.Cs, 27.50.+e

*Present address: U.S. Army Research Laboratory, Adelphi, Maryland 20783, USA
†Present address: Ernst & Young GmbH, Mergenthalerallee 3-5, 65760 Eschborn/Frankfurt (Main), Germany
‡Present address: TRIUMF, Vancouver, British Columbia V6T 2A3, Canada
§Present address: Patentanwälte Maikowski & Ninnemann, Kurfürstendamm 54-55, 10707 Berlin, Germany
¶Present address: Department of Physics and Astronomy, Rutgers University, Piscataway, New Jersey 08854-8019, USA
**Present address: Marshall Space Flight Center, Huntsville, Alabama 35812, USA
††Present address: CEA Saclay, Gif-sur-Yvette 91191, France
‡‡Present address: Department of Physics, University of Massachusetts Lowell, Lowell, Massachusetts 01854, USA
§§Present address: Department of Nuclear Engineering, University of California Berkeley, Berkeley, California 94720, USA
¶¶Present address: Department of Physics, University of Tokyo, Hongo, Bunkyo-ku, Tokyo 113-0033, Japan

## I. INTRODUCTION

The structure of neutron-rich nuclei in the vicinity of $^{68}$Ni has been the subject of considerable scrutiny in recent years, including investigations related to the magicity of $^{68}$Ni [1–10], the existence of multiple coexisting shapes [11–14], the presence of intruder states originating from orbitals across a shell gap [15–22], and the unexpected disappearance of seniority isomers [23–29]. The delineation of levels up to several MeV in excitation energy in these nuclei is an important step towards providing a firmer understanding of their properties through comparisons with modern theoretical models. Much of this effort has been concentrated thus far on $^{68}$Ni itself, with substantial improvements made to the level scheme [30–32] and deduced decay rates [12, 31], as well as with comparisons of the data with Monte-Carlo shell-model (MCSM) calculations [33, 34]. The latter have provided strong evidence for coexisting spherical, oblate, and prolate shapes in this nucleus [12, 13]. The calculated potential-energy surfaces in Ref. [13] also indicate

the likelihood of shape coexistence in $^{70}$Ni.

Most of what is known of the $^{70}$Ni level scheme comes from $\beta$-decay studies [26, 35] or from isomer tagging following fragmentation reactions [23–25]. In the latter works, a 232(1)-ns $(8^+)$ state, decaying via a four-transition cascade to the ground state, was identified at 2860 keV in $^{70}$Ni and attributed to a seniority isomer based on the $(\nu g_{9/2})^2$ configuration. The $\beta$-decay measurements added three more levels: A 1868-keV state was observed [26, 35] to decay by a 608-keV $\gamma$ ray to the 1260-keV $2_1^+$ level and, in Ref. [35] only, by a direct 1868-keV transition to the ground state. This state was assigned spin and parity $I^\pi = (2_2^+)$ [26, 35]. Both of these works identified a 683-keV $\gamma$ ray in the $\beta$ decay of the $(6^-, 7^-)$ $^{70}$Co isomer and placed it as feeding the 2679-keV $(6^+)$ level, resulting in a proposed 3362-keV $(7^-)$ state [26, 35]. Sawicka *et al.* additionally observed a 916-keV $\gamma$ ray that was assigned as the decay of a new 3146-keV $(5^-)$ state [26].

Although the yrast sequence could be reasonably well reproduced by shell-model calculations using a $^{56}$Ni core and a neutron $f_{5/2}pg_{9/2}$ model space, the $(5^-)$ and $(7^-)$ states, originating from excitations of negative-parity $fp$ neutrons across the $N = 40$ shell gap into the $g_{9/2}$ subshell, were found to be spaced several hundred keV more closely experimentally than predicted [26]. This suggested that there was an issue with cross-shell particle-hole excitations for the interactions used in the calculations. More problematically, calculations in such a model space were unable to reproduce a $2_2^+$ level located as low in energy as 1868 keV [36] (see also Sec. IV).

This paper presents results on the structure of $^{70}$Ni from the same data sets used in recent studies of $^{68}$Ni [30, 31]. As with $^{68}$Ni [12, 13, 31], the updated $^{70}$Ni level scheme is compared to shell-model calculations using interactions confined strictly to neutron excitations and to MCSM calculations employing a much larger model space, revealing better agreement for the negative-parity levels and insight into the nature of the non-yrast low-spin levels. These data provide a new test of the interactions relevant for the description of more exotic neutron-rich nuclei out to doubly-magic $^{78}$Ni and beyond and hint at a deeper understanding of their underlying structure.

## II. EXPERIMENTAL DETAILS

Excited states in $^{70}$Ni were populated in multinucleon-transfer reactions between a 440-MeV $^{70}$Zn beam and a $\sim$50-mg/cm$^2$ $^{208}$Pb target. The beam was provided by the ATLAS facility at Argonne National Laboratory in $\sim$0.3-ns-wide beam pulses delivered to target every 412 ns. The target, located at the center of the Gammasphere array of 100 Compton-suppressed high-purity Ge (HPGe) detectors [37], was sufficiently thick to stop all reaction products. Additional details of the experiment and analysis, including the sorting of $\gamma$ rays into prompt and delayed coincidence cubes and angular-correlation

matrices, with subsequent examination with the RAD-WARE analysis codes [38], are described in Ref. [30].

A complementary experiment employing secondary fragmentation reactions from a cocktail beam including predominantly $^{73}$Cu and $^{72}$Ni ions at the Coupled Cyclotron Facility of the National Superconducting Cyclotron Laboratory was also used to study excited states in $^{70}$Ni. Details of this experiment are provided in Ref. [31]. The $^{70}$Ni reaction products were identified on an event-by-event basis with the focal-plane detection system of the S800 spectrograph [39]. Prompt $\gamma$ rays associated with $^{70}$Ni events were detected with the high-resolution detector array GRETINA [40, 41], comprised of seven modules with four, 36–fold segmented HPGe crystals each, arranged around the target position of the S800 spectrometer. Decomposition of signals [41] generated by the detection of $\gamma$ rays emitted by the in-flight (velocity $v = 0.374c$) reaction products provided sub-segment position resolution for event-by-event Doppler reconstruction. Analysis of $\gamma$-ray-single and $\gamma\gamma$-coincidence events from GRETINA was performed with the RADWARE software package and its associated background-subtraction algorithms [38]. The $^{70}$Ni $\gamma$-ray spectra associated with secondary reactions from either $^{72}$Ni or $^{73}$Cu incident ions were found to be very similar; thus, the $^{70}$Ni data were combined irrespective of the incoming projectile.

## III. RESULTS

### A. Multinucleon-transfer reactions with Gammasphere

The yrast sequence of $^{70}$Ni had been previously delineated up to a 232-ns isomer at 2861 keV [24, 25], indicated in the level scheme in Fig. 1. Transitions have also been observed in the $\beta$ decay of $^{70}$Co that bypass this isomer [26, 35]. Thus, the analysis of the Gammasphere data proceeded using different combinations of prompt (P) and delayed (D) coincidence gates. A sum of double gates on each pair of the 1260-, 970-, and 448-keV transitions in the DDD cube produces the background-subtracted spectrum given in Fig. 2(a), where all three of these lines and the 183-keV isomeric transition can be seen. A spectrum double gated on the 1260- and 970-keV $\gamma$ rays in the PPP cube, Fig. 2(b), also demonstrates the expected coincidence with the 448-keV $\gamma$ ray. Additional peaks that have been associated here with $^{70}$Ni are also observed in this spectrum at 234, 483, 683, 1080, and 1113 keV and, more weakly, at 846 and 914 keV. The properties of these $\gamma$ rays are summarized in Table I.

A 683-keV transition was previously identified following the $\beta$ decay of $^{70}$Co and placed as feeding the 2678-keV level in Refs. [26] and [35]. The former work also reported a 916-keV line, possibly the same transition as the 914-keV $\gamma$ ray identified in the present data, which was tentatively assumed by Sawicka *et al.* to feed into the
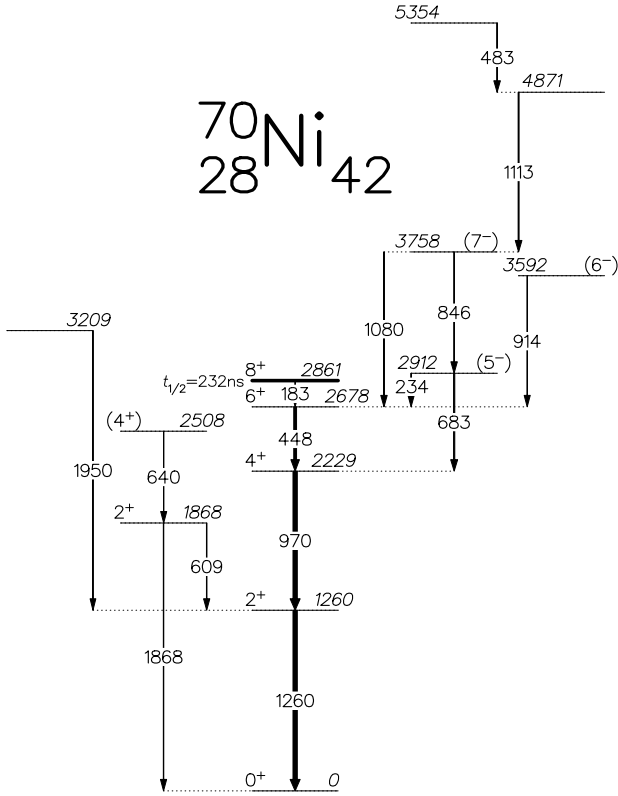
FIG. 1: Level scheme of $^{70}$Ni deduced from the multinucleon-transfer and secondary fragmentation reactions. The energies of $\gamma$ rays and states are given in keV. Spin-parity assignments in parentheses are tentative. The widths of the arrows represent the relative transition intensities. The half-life of the $8^+$ state is adopted from Ref. [25].



FIG. 2: Background-subtracted, double-gated $\gamma$-ray coincidence spectra recorded with Gammasphere following $^{70}$Zn + $^{208}$Pb multinucleon-transfer reactions. (a) Sum of double gates on each pair of the 1260-, 970-, and 448-keV transitions in the delayed data. (b-e) Double gates in the prompt data on (b) 1260 and 970 keV, (c) 448 keV with either 1260 or 970 keV, (d) 1080 keV with either 1260 or 970 keV, and (e) one gate on 1260 or 970 keV and the other on 234 or 683 keV. Peaks assigned to $^{70}$Ni are labelled with their $\gamma$-ray energies in keV. Transitions that appear weakly in a given panel, but were found to have supporting evidence from other coincidence gates, are labelled in parentheses.

2229-keV level in parallel to the 448-keV transition. In the Gammasphere PPP data, a double gate on the 448-keV and either the 1260- or 970-keV transitions yields the spectrum in Fig. 2(c). The 683-keV line seen in Fig. 2(b) disappears in this spectrum, whereas the other lines (apart from the 448-keV gate), including the peak at 914 keV, remain. This indicates that all of the newly identified $\gamma$ rays feed into the yrast sequence above the 2678-keV state with the exception of the 683-keV transition, which instead decays to the 2229-keV level. This is contrary to the placements of the 683- and 916-keV transitions in Refs. [26, 35]. The presence of a 234-keV $\gamma$ ray in these spectra supports the modified placement of the 683-keV transition depopulating a level at 2912 keV, as the energy sums and coincidence relationships indicate that the former decays from the same state (see Fig. 1).

Figure 2(d) presents a Gammasphere coincidence spectrum double gated on the transitions at 1080 keV and either 1260 or 970 keV. The 234- and 683-keV lines are absent in this gate. The 1080-, 1113-, and 483-keV $\gamma$ rays are found to be in mutual coincidence, and are placed in a cascade directly feeding the 2678-keV state (Fig. 1). A weak 846-keV line is observed in the spectrum dou-
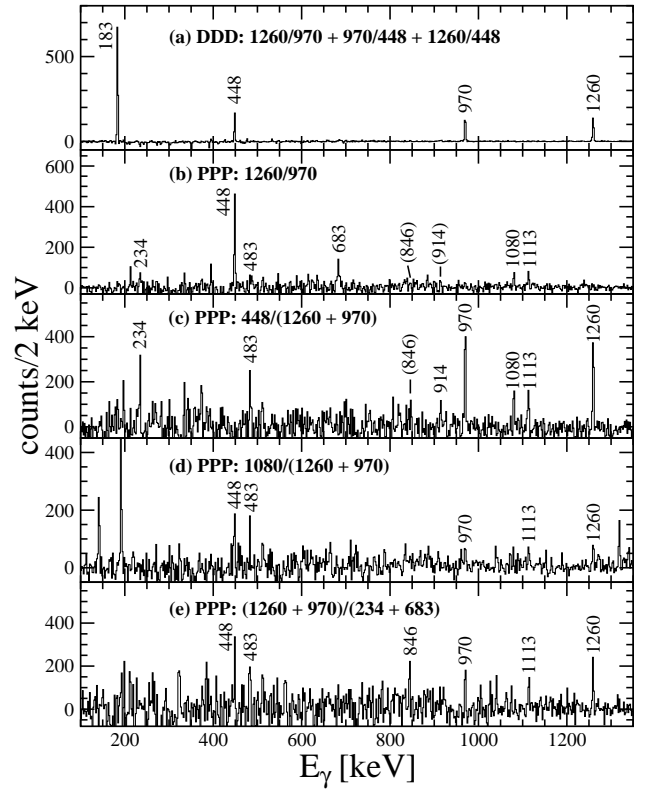
ble gated on either 1260 or 970 keV and either 234 or 683 keV, Fig. 2(e), as well as in the spectra of Figs. 2(b) and 2(c). The relatively poor peak-to-background ratio for the 846-keV transition can be attributed, at least in part, to the subtraction of a large background around this energy. This transition can be consistently placed between the 3758- and 2912-keV states, and explains the observation of the 1113- and 483-keV $\gamma$ rays in the spectrum of Fig. 2(e).

Levels above the 2861-keV isomer were sought in the PDD and PPD subsets of the data as was done in, e.g., Refs. [30, 42], but without success. In particular, none of the states identified for the first time in this work were found to decay into the isomer.

Although the 2861-keV isomer has been assumed since its initial discovery to be an $(8^+)$ state [24], only the spin and parity of the 1260-keV $2^+$ state had been previously established experimentally, in the Coulomb-excitation

TABLE I: Properties of $\gamma$ rays in $^{70}$Ni identified with Gammasphere following multinucleon-transfer reactions. The efficiency-corrected relative intensities $I_\gamma$ were determined from the $\gamma\gamma\gamma$ prompt coincidence data and normalized to 100 for the 448-keV transition. The excitation energy $E_x$ for the level depopulated by each $\gamma$ ray is given in the third column. The last column provides the spin-parity assignments for the initial and final levels.

| $E_\gamma$ (keV) | $I_\gamma$ | $E_x$ (keV) | $I_i^\pi \to I_f^\pi$ |
|---|---|---|---|
| 183.11(2)[a] | | 2860.9(2) | $8_1^+ \to 6_1^+$ |
| 234.1(1) | 16.5(17) | 2912.0(2) | $(5_1^-) \to 6_1^+$ |
| 448.37(3)[a] | 100(5) | 2677.8(1) | $6_1^+ \to 4_1^+$ |
| 482.9(2) | 29(6) | 5354.4(8) | |
| 683.1(2) | 43(4) | 2912.0(2) | $(5_1^-) \to 4_1^+$ |
| 846(1) | 24(12) | 3758.1(6) | $(7_1^-) \to (5_1^-)$ |
| 914.4(3) | 12(4) | 3592.2(6) | $(6_1^-) \to 6_1^+$ |
| 969.88(4)[a] | | 2229.4(1) | $4_1^+ \to 2_1^+$ |
| 1080.3(3) | 24(3) | 3758.1(6) | $(7_1^-) \to 6_1^+$ |
| 1113.4(2) | 34(5) | 4871.5(7) | $\to (7_1^-)$ |
| 1259.52(5)[a] | | 1259.5(1) | $2_1^+ \to 0_1^+$ |

[a]Energy measured in delayed spectrum.



FIG. 3: (Color online) Angular correlations for members of the $^{70}$Ni yrast sequence gated on the coincident 1260-keV $2^+ \to 0^+$ transition in the delayed Gammasphere data. The expected curve for an $E2 - E2$ correlation is also plotted, scaled to each set of measurements.

measurement of Ref. [43]. To address this issue, an angular-correlation (AC) analysis was performed using a DD subset of the Gammasphere data. AC matrices were constructed as described in Ref. [30] and combined into average angle groups at 20.3°, 37.5°, 55.4°, 71.4°, and 85.2°. A gate was placed on the delayed 1260-keV $2^+ \to 0^+$ transition and the relative intensities (with appropriate efficiency corrections) of the coincident 970-, 448-, and 183-keV $\gamma$ rays were determined at each angle. The results are plotted in Fig. 3 along with the theoretical curve for an $E2 - E2$ correlation, scaled to each set of data. The data are consistent with $E2$ multipolarities in all three cases. (In contrast, if they had been stretched dipoles, the AC curves would be positively sloped.) Thus, the spin-parity assignments in the yrast sequence up to the $8^+$ isomer are confirmed.

An AC analysis was attempted in the prompt data for the $\gamma$ rays feeding into the yrast sequence at the $4^+$ level and above, but no reliable results could be obtained for these weaker lines. Other arguments can be used to tentatively propose spins and parities, however. The 683- and 914-keV transitions were both observed in the $\beta$ decay of the $^{70}$Co ground state [26, 35], which is expected to have spin-parity $I^\pi = 6^-$ or $7^-$, based on shell-model considerations. Under the assumption of direct $\beta$ feeding to the 2912- and 3592-keV states in $^{70}$Ni, negative-parity assignments for both are favored. As the former decays to a $4^+$ and a $6^+$ level, it can likely be assigned $I^\pi = (5^-)$. Both the 3592- and 3758-keV levels feed the $6^+$ member of the yrast sequence, with the latter also populating the $(5^-)$ state, suggesting that one of them has $I^\pi = (6^-)$ quantum numbers and the other $I^\pi = (7^-)$. The choice of assignments indicated in Fig. 1 has been guided by
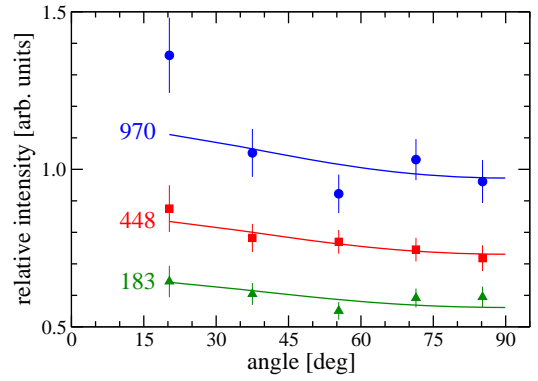
shell-model calculations (see Sec. IV), as there is insufficient evidence for an experimental determination.

In a more recent examination of the $\beta$ decay of $^{70}$Co [44], observation of a 233-keV $\gamma$ ray motivated the similar placement of a 681-keV transition feeding the yrast $4^+$ state from a new $(5^-)$ level at 2913 keV; a 916-keV $\gamma$ ray was also placed directly above the $6^+$ state based on limited coincidence events, with a second line at 683 keV proposed to decay parallel to it. These modified levels were subsequently included without discussion in Fig. 2 of Ref. [45]. The present data do not support the claims of a ~683-keV doublet: the second line is not seen in the appropriate coincidence spectra [e.g., Fig. 2(c)] and the branching ratio for the 234- and 683-keV transitions in these two studies only agree if the 683-keV $\gamma$ ray is a single line.

It is worth adding that, using the intensities quoted in the earlier $\beta$-decay studies [26, 35] with the current arrangement of the level scheme, the net $\beta$-feeding intensity into the 2229-keV $4^+$ level is consistent with zero. This observation aids in assigning spins to other states in the next section.

## B. Secondary fragmentation reactions with GRETINA

The data from the secondary reactions are, to a large extent, complementary to those from the multinucleon-transfer experiment. This is evident in the Doppler-corrected $\gamma$-singles spectrum for the former, given in Fig. 4(a), where the peaks at 1259(1) and 968(1) keV are the only ones common to both data sets, corresponding to the 1259.5- and 969.9-keV lines (Table I). A transition at 608 keV had been previously identified in the $\beta$-decay works of Mueller et al. [35] and Sawicka et al. [26], placed decaying from a 1868-keV level to the one at 1260 keV. The former study additionally observed a 1868-keV

crossover transition directly to the ground state [35]; the absence of this $\gamma$ ray in the latter work was attributed to the weak population of the state in that measurement [26]. Peaks at 609 and 1868 keV are clearly visible in the GRETINA singles spectrum in Fig. 4(a), confirming their assignment to $^{70}$Ni. The remaining five transitions indicated in this figure were not observed in either multinucleon transfer (this work) or following $\beta$ decay [26, 35]. The properties of these $\gamma$ rays are summarized in Table II.
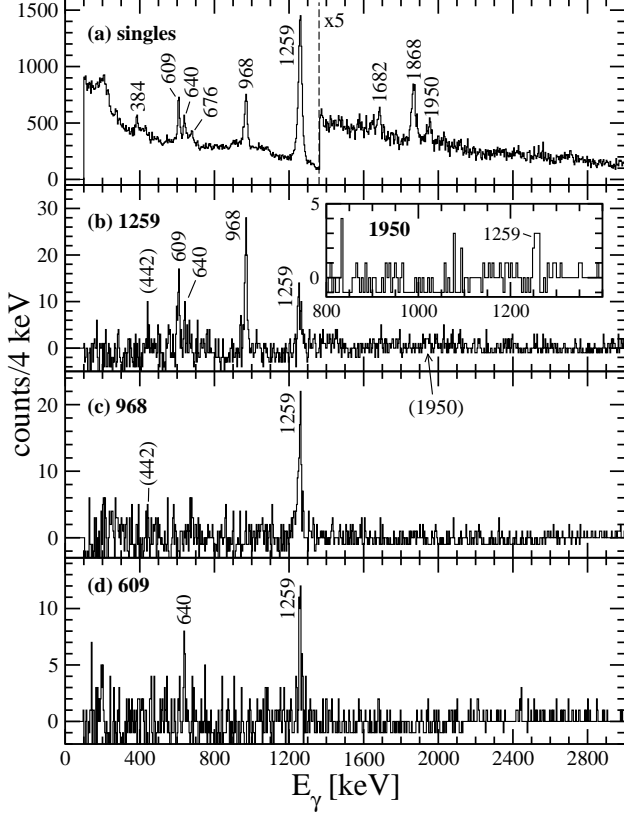


FIG. 4: Prompt $\gamma$ rays recorded with GRETINA in coincidence with $^{70}$Ni recoils following secondary reactions, Doppler corrected for $v/c = 0.374$. (a) Singles spectrum. (b-d) Background-subtracted coincidence spectra gated on (b) 1259, (c) 968, (d) 609, and (b inset) 1950 keV.

The background-subtracted, Doppler-corrected GRETINA spectrum coincident with the 1259-keV line is given in Fig. 4(b). The expected peaks at 968 and 609 keV are visible, and there is evidence for the line at 640 keV that can also be found in the singles spectrum [Fig. 4(a)]. The 1259-keV transition is self-coincident, as a gate at this energy brings back a peak at a similar position; this may correspond to the 1259.6- and 1256.8-keV pair identified in the $\beta$ decay of the low-spin $^{70}$Co isomer in Ref. [35]. Peaks this closely spaced would not be resolved in the present data, so the energy of the 1256.8-keV member of the doublet is adopted from Ref. [35] and reported in Table II.

TABLE II: Properties of $\gamma$ rays in $^{70}$Ni identified with GRETINA following secondary reactions. The efficiency-corrected relative intensities $I_\gamma$ were determined from the singles spectrum and normalized to 100 for the strongest transition. The excitation energy $E_x$ for the level depopulated by each $\gamma$ ray is given in the third column; for cases without an entry, there are insufficient coincidence data to place the transition. The last column provides the spin-parity assignments for the initial and final levels. See text regarding the entry for the 1256.8-keV transition.

| $E_\gamma$(keV) | $I_\gamma$ | $E_x$ (keV) | $I_i^\pi \to I_f^\pi$ |
|---|---|---|---|
| 384(1) | 3.8(4) | | |
| 609(1) | 12.3(6) | 1868(1) | $2_2^+ \to 2_1^+$ |
| 640(1) | 8.1(5) | 2508(1) | $(4_2^+) \to 2_2^+$ |
| 676(1) | 4.7(5) | | |
| 968(1) | 27(3) | 2227(1) | $4_1^+ \to 2_1^+$ |
| 1256.8$^a$ | | *2516.4* | $(0_3^+, 2_3^+) \to 2_1^+$ |
| 1259(1) | 100(10) | 1259(1) | $2_1^+ \to 0_1^+$ |
| 1682(2) | 3.5(6) | | |
| 1868(1) | 11.2(7) | 1868(1) | $2_2^+ \to 0_1^+$ |
| 1950(2) | 4.2(6) | 3209(2) | $\to 2_1^+$ |

$^a$Energy taken from Ref. [35].

Although this transition cannot be placed with certainty in the $^{70}$Ni level scheme based on the GRETINA data alone, the fact that the coincident 1260- and 1257-keV $\gamma$ rays were both observed in the $\beta$ decay of the low-spin $^{70}$Co isomer, but the 970-keV transition was not [35], suggests the presence of a low-spin state at 2516.4 keV in $^{70}$Ni depopulated by the 1256.8-keV $\gamma$ ray to the $2_1^+$ level. As this decay is prompt, only dipole or quadrupole transitions are expected, limiting the spin of the 2516-keV level to $I \leq 4$. Based on shell-model calculations, the presence of a state with spin 1 or 3 at such a low excitation energy appears unlikely, considering the orbitals available near the Fermi surface (see discussion below). Furthermore, the absence of any observed $\beta$ feeding to $4^+$ states argues against a $4^+$ assignment here. Therefore, this state is tentatively assigned $I^\pi = (0^+)$ or $(2^+)$. Direct feeding of a $0^+$ state would not be expected from a $3^+$ $\beta$-decay parent, as assigned by Mueller *et al.* [35]. However, the latter was based on systematics of $\beta$-decaying isomers in the lighter Co isotopes, and recent studies have suggested that the original assignment of $I^\pi = (3^+)$ in $^{68}$Co [35] should be changed to $(1^+)$ [17] or to $(2^-)$ [46]. In light of this controversy, the spin of the $^{70}$Co isomer will also require further evaluation.

The weak $\gamma$ ray at 442(5) keV, visible only in the coincidence data [Fig. 4(b)], might correspond to the known 448-keV $6^+ \to 4^+$ transition of the yrast sequence. The 1950-keV peak seen in singles is also found, rather weakly, in the 1259-keV coincidence gate; the inset of Fig. 4(b) provides the spectrum gated on this 1950-keV line, in which a concentration of counts at 1259 keV can be seen,

confirming this coincidence.

Figure 4(c) provides the background-subtracted, Doppler-corrected GRETINA spectrum gated on 968 keV, in which the expected peak at 1259 keV is seen. The 609- and 1950-keV $\gamma$ rays found to be coincident with the 1259-keV line [Fig. 4(b)] are absent in this spectrum, indicating that these two transitions feed into the yrast sequence at the $2^+$ level. Finally, the background-subtracted spectrum gated on 609 keV in Fig. 4(d) demonstrates the mutual coincidence of the 640-, 609-, and 1259-keV transitions. With the 609-keV $\gamma$ ray depopulating a level at 1868 keV, as proposed in Refs. [26, 35], the 640-keV transition is placed directly above this state, consistent with the relative intensities of the two lines.

The 1868-keV state $\gamma$ decays directly to the ground state, ruling out the possibility of a $0^+$ assignment for the former level. As noted above, low-lying states with spin 1 or 3 are not expected. Thus, an assignment of $I^\pi = 2^+$ is adopted, in agreement with Ref. [35]. The 2508-keV level does not appear to feed the ground state directly, with only a transition to the $2_2^+$ state having been observed, and is not fed in $\beta$ decay as the $2_{1,2}^+$ states are. These observations suggest that it is likely not another $2^+$ level and, therefore, a tentative $(4^+)$ assignment is proposed. This assignment is consistent with the earlier observation that the established $4^+$ level at 2229 keV is not fed in the $\beta$ decay of either $^{70}$Co isomer. However, in view of the uncertain spin and parity of the low-spin isomer, a $0^+$ assignment cannot be completely ruled out. Note that the 640-keV $(4_2^+) \to 2_2^+$ transition energy here is quite similar to the 662-keV decay between corresponding states in $^{68}$Ni [30, 32].

It should be emphasized that the secondary reactions are found to strongly populate only low-spin levels, with little or no evidence that transitions known to decay from states with spin $I > 4$ have been observed in the GRETINA spectra.
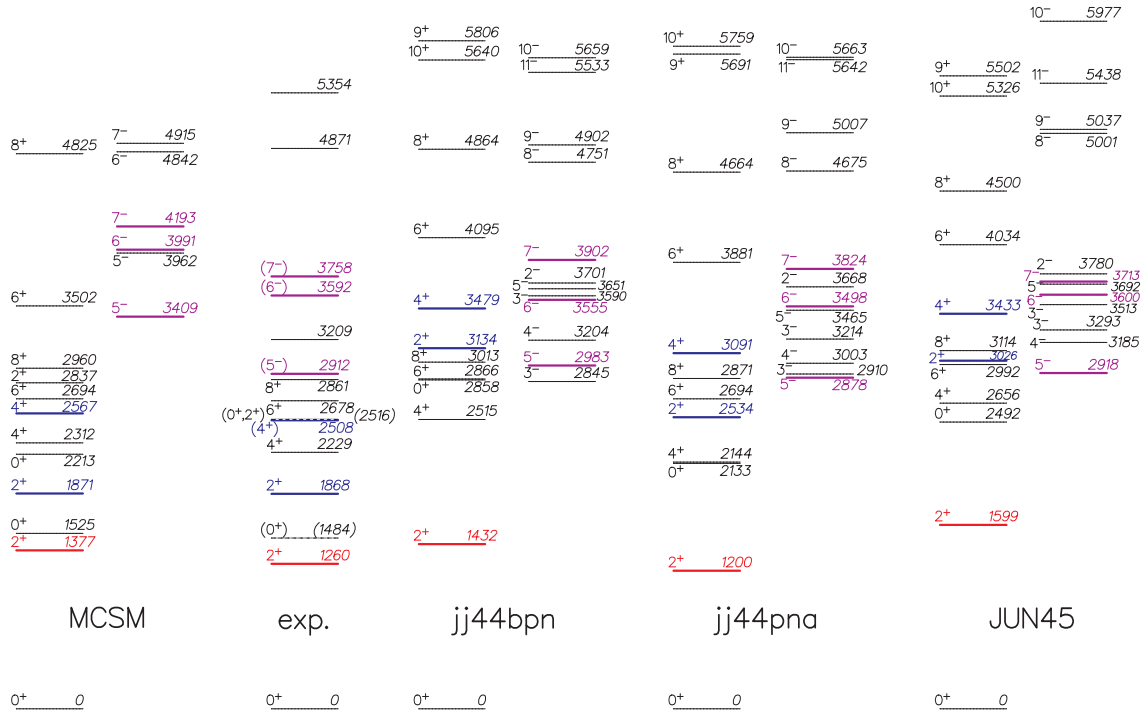
## IV. DISCUSSION

The levels in the $^{70}$Ni decay scheme given in Fig. 1 fall into three groups: the yrast sequence up to the $8^+$ isomer; a set of negative-parity states at higher excitation energies (right side of Fig. 1); and non-yrast, low-spin, positive-parity levels (left side). At $Z = 28$, the proton Fermi surface is situated well within the negative-parity $fp$ shell, while there must be at least two neutrons occupying the positive-parity $g_{9/2}$ orbital above $N = 40$. The yrast sequence is dominated by the $\nu g_{9/2}^2$ configuration that has received considerable attention recently in light of the surprising disappearance of the so-called seniority isomers in the Ni isotopes in the middle of the $g_{9/2}$ shell [23–29]. In order to generate negative-parity levels, an odd number of neutrons must be excited out of the $fp$ shell into the $g_{9/2}$ orbital. Generally speaking, in the simplest scenario, a neutron hole in a $p_{1/2}$, $f_{5/2}$, or $p_{3/2}$ orbital can couple to the $g_{9/2}$ particle, with the remaining $g_{9/2}^2$ neutrons paired to zero, producing multiplets of negative-parity states with spins as high as $7\hbar$. By breaking the paired $g_{9/2}$ neutrons, an additional $6\hbar$ can be achieved. Higher-spin states could also be generated by promoting additional neutrons across the $N = 40$ gap or by breaking the proton core.

In Fig. 5, the experimental levels in $^{70}$Ni are compared to shell-model (SM) calculations including those performed with the ANTOINE [47] and/or NuShellX [48] codes using the jj44bpn [49], jj44pna [50], and JUN45 [51] effective interactions. For all three interactions, the model space is comprised of the neutron $p_{3/2}$, $f_{5/2}$, $p_{1/2}$, and $g_{9/2}$ orbitals outside of a $^{56}$Ni core. The same orbitals for protons are also included in these interactions, but do not play a role for the Ni isotopes; in this constrained valence space, proton excitations out of the closed $f_{7/2}$ subshell at $Z = 28$ are not considered.

In the $^{70}$Ni level scheme proposed by Sawicka et al. [26], the $(5^-)$ and $(7^-)$ states were placed at 3146 and 3362 keV, respectively, separated by 216 keV. This energy difference is considerably smaller than that predicted by the calculations using the jj44bpn (919 keV), jj44pna (946 keV), and JUN45 (795 keV) interactions. However, the rearrangement of the 683- and 914-keV transitions in the present work, as well as the addition of the 1080-keV $\gamma$ ray from a state at 3758 keV, result in an energy separation of 846 keV, bringing all three calculations into better agreement with experiment. In particular, the measured energies of the $(5^-)$, $(6^-)$, and $(7^-)$ levels (colored purple in the online version of Fig. 5) are reproduced to within 100 keV, with the exception of the $7^-$ state for the jj44bpn interaction (144 keV).

The experimental levels at 4871 and 5354 keV have not been assigned spin and parity but, based on the expectation that multinucleon-transfer reactions predominantly populate states near the yrast line, they are assumed to have $I > 7$. As noted earlier, spins larger than $7\hbar$ necessarily involve configurations with additional active nucleons. The 4871-keV level is similar in energy to both the $8^-$ and $9^-$ states in the jj44bpn, jj44pna, and JUN45 calculations, originating from the breaking and recoupling of the $\nu g_{9/2}^2$ pair. The $8_2^+$ level, formed from an additional parity-changing cross-shell neutron excitation, is also predicted to be near this energy, especially with the jj44bpn interaction. The observed level is found to decay to the $(7^-)$ state, but not the $(6^-)$ one, which would favor either a $(9^-)$ or $(8^+)$ assignment. The 5354-keV state, decaying to the 4871-keV level via the 483-keV transition, can be energetically matched with calculated $9^+$, $10^+$, $10^-$, or $11^-$ states, partly depending on the interaction used, any of which would be consistent with the deduced level scheme. Thus, the data are insufficient to constrain these assignments further. Regardless of the assignment, however, there is generally satisfactory agreement between the measured energies of the high-spin states and the predictions of the three sets of calculations involving only neutron excitations.
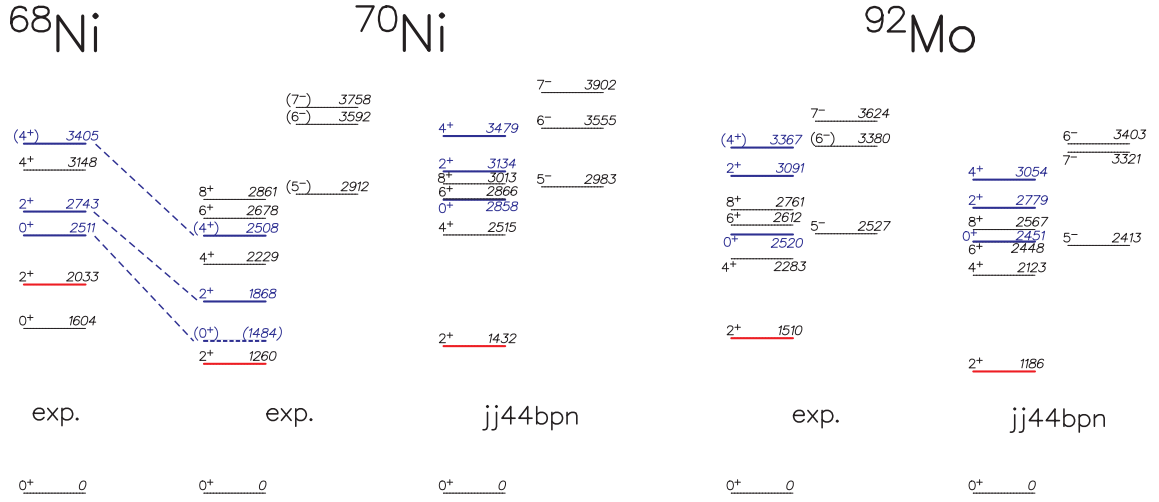
FIG. 5: (Color online) Experimental levels (exp.) in $^{70}$Ni compared with shell-model calculations using a number of effective interactions in the neutron $f_{5/2}pg_{9/2}$ model space (jj44bpn, jj44pna, and JUN45) and MCSM calculations using the A3DA interaction in the full $fpg_{9/2}d_{5/2}$ space for both protons and neutrons. A tentative $(0_2^+)$ level is drawn for $^{70}$Ni based on the scenario discussed in the text of a 384-keV decay from the 1868-keV $2^+$ state.

The success of these calculations at reproducing the negative-parity states does not, however, carry over to the low-spin, positive-parity levels. In particular, while the $2_1^+$ state (red in the online version of Fig. 5) can be reasonably well reproduced, the predicted $2_2^+$ and $4_2^+$ states (in blue) differ by 0.6 to 1.3 MeV from the observed ones at 1868 and 2508 keV, respectively. This can be viewed as a strong indication for a missing ingredient in the calculations related to these particular states. Naturally, proton excitations come to mind, as these were excluded from the calculations discussed thus far.

Support for this hypothesis can be found in a comparison of the level schemes of $^{70}_{28}$Ni$_{42}$ and its valence-mirror nucleus $^{92}_{42}$Mo$_{50}$. (While $^{70}$Ni has 42 neutrons and a closed proton shell, $^{92}$Mo, conversely, has 42 protons and a closed neutron shell.) Figure 6 provides partial experimental level schemes for both nuclei along with SM calculations for each using the jj44bpn interaction. For clarity, only the lowest two $0^+$, $2^+$, and $4^+$ levels and the yrast $6^+$, $8^+$, $5^-$, $6^-$, and $7^-$ states are shown. With the same nucleon number, excitations within the neutron system for $^{70}$Ni and that of the protons for $^{92}$Mo are expected to be similar and can thus be treated by these calculations in the corresponding $f_{5/2}pg_{9/2}$ model spaces. Indeed, the experimental and theoretical yrast $2^+$, $4^+$, $5^-$, $6^-$, and $7^-$ states, all dominated by excitations into the $g_{9/2}$ subshell (i.e., within the model space),

are in similar agreement. On the other hand, the calculated $0_2^+$, $2_2^+$, and $4_2^+$ levels (blue in the online version of Fig. 6) are significantly elevated in $^{70}$Ni compared to the data while, in $^{92}$Mo, both the experimental and theoretical energies for the corresponding states are elevated and in better agreement. As stated above, the $f_{5/2}pg_{9/2}$ model space used in these calculations excludes excitations across $Z = 28$ for $^{70}$Ni, and across $N = 50$ for $^{92}$Mo. The observations above then lead to the conclusion that the $N = 50$ shell gap is sufficiently large to preclude the presence of neutron particle-hole excitations at relatively low excitation energies, but that, in contrast, the $Z = 28$ gap is insufficient to prevent the corresponding proton excitations. Hence, such proton particle-hole excitations that lie outside the scope of the calculations discussed thus far will now be considered.

The spectrum of states in $^{70}$Ni was calculated with the Monte-Carlo shell model (MCSM) using the A3DA interaction [33]. Here, the full $fpg_{9/2}d_{5/2}$ model space for both protons and neutrons was employed, allowing for the breaking of the $\pi f_{7/2}$ shell below $Z = 28$. This is part of the same series of calculations as recently reported by Suchyta et al. [12] that successfully described the low-lying level structure of $^{68}$Ni. Figure 3 of Ref. [13] presented the potential-energy surface (PES) for $^{68}$Ni as a function of quadrupole moment (deformation), wherein spherical, oblate, and prolate minima were identified; the

FIG. 6: (Color online) Experimental levels (exp.) in $N = 42$ $^{70}$Ni and the valence-mirror nucleus $Z = 42$ $^{92}$Mo compared with shell-model calculations using the jj44bpn effective interaction. The data for $^{92}$Mo are taken from Ref. [52]. A tentative $(0_2^+)$ level is drawn for $^{70}$Ni based on the scenario discussed in the text of a 384-keV decay from the 1868-keV $2^+$ state. Experimental levels in $^{68}$Ni are also shown, with dashed lines to their counterparts in $^{70}$Ni indicating the trend of decreasing excitation energies for levels associated with prolate deformation.

PES is also given here in Fig. 7(a). A modest potential barrier separates the prolate minimum from the other two, whereas there is only a negligible one between the oblate and spherical minima. The main configuration components for the $0_1^+$ ground, $0_2^+$, and $0_3^+$ states in $^{68}$Ni were found to be associated with, respectively, the spherical, oblate, and prolate potential minima, as indicated in Figs. 3(a) to 3(c) of Ref. [13].

prolate deformation [Figs. 8(b), 8(e), and 8(h)], with a quadrupole moment similar to that of the prolate minimum in $^{68}$Ni. Although the PESs are qualitatively similar for $^{68}$Ni [Fig. 7(a)] and $^{70}$Ni [Fig. 7(b)], the local prolate minimum in $^{70}$Ni is deeper relative to the spherical one than is the case in $^{68}$Ni. Consequently, the levels associated with the prolate minimum are expected to come down lower in excitation energy in $^{70}$Ni.



FIG. 7: (Color online) Potential-energy surfaces for (a) $^{68}$Ni and (b) $^{70}$Ni as a function of quadrupole deformation, obtained from constrained Hartree-Fock calculations for the A3DA Hamiltonian.

The shapes associated with states in $^{70}$Ni have been similarly calculated and are plotted for the $0_{1,2,3}^+$, $2_{1,2,3}^+$, and $4_{1,2}^+$ levels in Fig. 8. In these plots, circles represent the overlap between the wave function for a specific state (indicated by its spin and parity in each panel) and the basis states having quadrupole moments $Q_0$ and $Q_2$. At $N = 42$, the $^{70}$Ni ground state involves at least two neutrons occupying the $g_{9/2}$ orbital and is found in the MCSM calculations to tend towards a spherical to slightly oblate shape, as do the $2_1^+$ and $4_1^+$ states [Figs. 8(a), 8(d), and 8(g)]. In contrast, the $0_2^+$, $2_2^+$, and $4_2^+$ states are predicted to be associated with a sizable
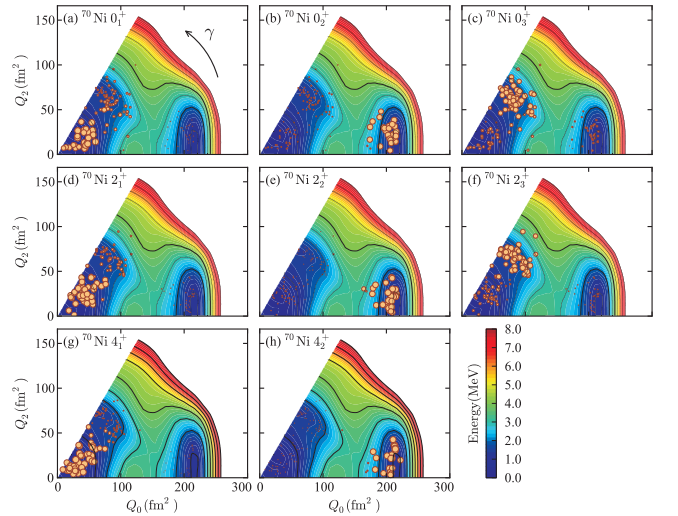


FIG. 8: (Color online) Potential-energy surfaces for $^{70}$Ni as a function of quadrupole deformation, obtained from constrained Hartree-Fock calculations for the A3DA Hamiltonian. Circles represent the size of the overlap between the wave function calculated for a given level, indicated by its spin and parity on each panel, and the basis states having quadrupole moments $Q_0$ and $Q_2$.

The $^{70}$Ni level scheme resulting from the MCSM calculations is presented on the left side of Fig. 5. The positive-parity levels are found to be in good agreement with the experimental values; in particular, the calculated $2_2^+$ and $4_2^+$ states differ by 3 and 61 keV, respectively, from their measured counterparts, a considerable improvement over the shell-model calculations restricted to neutrons only, discussed earlier. As anticipated from the calculated depths of the potential wells, the $2_2^+$ state in $^{70}$Ni is, indeed, lower than the one in $^{68}$Ni—at 1868 keV compared to 2743 keV. The prolate $0^+$ level is also expected lower in energy than in $^{68}$Ni, predicted by the MCSM calculations to lie fairly close to the $2_1^+$ state. This level was not firmly identified in the present work. However, two $\gamma$ rays, with energies 384 and 676 keV, were observed in the singles spectrum from the secondary fragmentation experiment [see Fig. 4(a)], but not placed in the level scheme due to a lack of sufficient coincidence information. The presence of these transitions in the fragmentation data, but not in the multinucleon-transfer experiment, indicates that they likely originate from low-spin states. If the 384-keV (or, to a lesser extent, the 676-keV) $\gamma$ ray depopulates the 1868-keV $2_2^+$ state, it would place the $0_2^+$ level at 1484 (or 1192) keV, consistent with the predicted energy of 1525 keV. A 1484-keV $0_2^+$ level is, thus, drawn tentatively in Figs. 5 and 6. In $^{68}$Ni, the $0_2^+$ level, at 1604 keV, is the first excited state and can only decay by an isomeric $E0$ transition to the $0_1^+$ ground state, proceeding via internal conversion [12] or pair production [12, 31]; the latter decay mode was identified with the same data sets as in the present work through the observation of delayed 511-keV annihilation $\gamma$ rays [31]. A similar search here did not reveal any delayed 511-keV lines correlated with $^{70}$Ni recoils, but the energy of the $0_2^+$ state may put the corresponding $E0$ transition too close to the pair-production threshold for there to be any substantial probability for this process to occur. Experimental confirmation of its position awaits a new, dedicated measurement. The lowering of the proposed prolate-deformed states in $^{70}$Ni compared to $^{68}$Ni is indicated on the left side of Fig. 6.

Although absolute $B(E2)$ transition strengths have not been determined in this work, the ratio of these values for parallel $E2$ decays out of a given level can be calculated and compared to theoretical predictions, as was done for $^{68}$Ni [31]. In particular, the possible 384-keV $2_2^+ \rightarrow 0_2^+$ decay can be compared to the 1868-keV transition to the ground state. The ratio $B(E2; 2_2^+ \rightarrow 0_2^+)/B(E2; 2_2^+ \rightarrow 0_1^+)$ deduced from the data is $9(1) \times 10^2$, compared to the value $4 \times 10^2$ from the MCSM calculations. These values agree to within a factor of about 2.5, demonstrating additional consistency for the tentative placement of the $0_2^+$ level at 1484 keV.

The tentatively assigned $(0_3^+, 2_3^+)$ level at 2516 keV lies about 300 keV away from both the predicted $0_3^+$ and $2_3^+$ states from the MCSM calculations. There is no clear preference for one spin assignment over the other. In either case, the calculations indicate an underlying

oblate shape for this state, as seen in Figs. 8(c), and 8(f). Thus, there is evidence of coexistence of (near) spherical, oblate, and prolate shapes at low excitation energies in $^{70}$Ni, as has also been demonstrated in $^{68}$Ni [12, 13, 31].

Prolate-deformed states similar to those in $^{68,70}$Ni have not yet been identified as such, either experimentally or theoretically, in $^{72}$Ni. In Ref. [45], a $(4_2^+)$ level was observed at 2164 keV following $\beta$ decay and interpreted in the context of seniority-conserving and -changing transitions between states based on excitations within the $g_{9/2}$ neutron shell. The lowering of seniority-4 levels such that fast, seniority-changing transitions may occur has been put forth as an explanation for the disappearance of isomerism in $^{72,74}$Ni [27]. The calculations describing these scenarios have typically excluded the $f_{7/2}$ proton subshell and, hence, excitations across the $Z = 28$ shell gap are forbidden in the given model spaces (see, e.g., Ref. [29] and therein). In light of the current work, an alternate explanation for the origin of the 2164-keV $4^+$ state in $^{72}$Ni is that it may be a member of a prolate-deformed proton-intruder sequence, even lower in excitation energy than its counterpart in $^{70}$Ni. Note also that the 579- and 699-keV transitions observed in Ref. [45], but not placed in the $^{72}$Ni level scheme, could both be potential candidates for a $2_2^+ \rightarrow 2_1^+$ transition, comparable in energy to the corresponding 609-keV $\gamma$ ray in $^{70}$Ni. If so, this could again represent an intruder state, lowered in energy from its position in $^{70}$Ni. Clearly, more data on $^{72}$Ni are required to investigate these possibilities.

The calculated $0_2^+$, $2_2^+$, $4_2^+$, and $6_2^+$ levels have all been found in this work to be dominated by configurations within the prolate well of the PES [Figs. 8(b), 8(e), and 8(h)]. As noted in Ref. [13] for $^{68}$Ni, this prolate minimum is associated with particle-hole excitations across *both* the $N = 40$ and $Z = 28$ shell gaps, primarily promoting neutrons from the $f_{5/2}$ and $p_{1/2}$ orbitals to the $g_{9/2}$ subshell and protons from the $f_{7/2}$ to the $p_{3/2}$, $f_{5/2}$, and $p_{1/2}$ orbitals (i.e., Type II shell evolution, see Ref. [13]). The situation for $^{70}$Ni is similar, as exemplified by the proton and neutron occupancies for the $0_{1,2}^+$ levels given in Figs. 9(a) and 9(b), respectively. Here, at $N = 42$, the occupation of at least a pair of $g_{9/2}$ neutrons even in the ground state reduces the size of the $\pi f_{7/2} - f_{5/2}$ gap through the tensor interaction [53], such that a prolate shape similar to that in $^{68}$Ni can be achieved at a smaller cost in excitation energy. This gap decreases further as neutron particle-hole excitations fill additional $g_{9/2}$ levels, see Fig. 9(c). Thus, the states in the prolate potential minimum form an intruder structure at low energy comparable to those found in the well-known cases of the Sn and Pb regions [13, 22, 54].

## V. CONCLUSIONS

To summarize, the level scheme of $^{70}$Ni has been extended both at low spins, using data from secondary fragmentation reactions with the GRETINA array, and
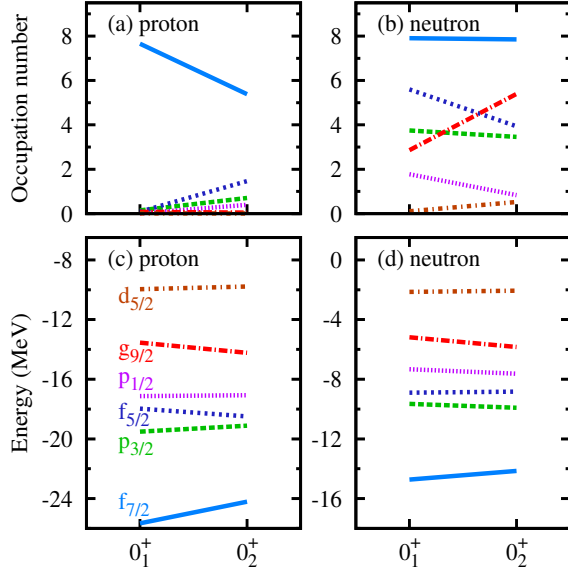
FIG. 9: (Color online) Occupancies and energies of proton and neutron orbitals near the Fermi surface for the $0_{1,2}^+$ levels in $^{70}$Ni. The same line styles are used in all panels, as labelled in (c).

at higher spins, following multinucleon-transfer reactions measured with the Gammasphere array. The spins and parities of the yrast sequence up to the $8^+$ isomer have been verified. The rearranged and newly added higher-spin states, with likely negative parity, are in good agreement with shell-model calculations employing effective interactions confined to neutron excitations in the $f_{5/2}pg_{9/2}$ model space. The previously known $2_2^+$ and new $(4_2^+)$ states are poorly reproduced by such calculations, however, and require the involvement of pro-

ton particle-hole excitations. Monte-Carlo shell-model calculations in a full $fpg_{9/2}d_{5/2}$ model space for both protons and neutrons provide better agreement with the data for these states and indicate that they reside within a prolate-deformed potential minimum. Thus, $^{70}$Ni is found to exhibit shape coexistence, similar to $^{68}$Ni, but with the prolate structure appearing at even lower excitation energy due to the presence of additional $g_{9/2}$ neutrons affecting the $Z = 28$ shell gap through the tensor interaction.

[1] R. Broda *et al.*, Phys. Rev. Lett. **74**, 868 (1995).
[2] M. Hannawald *et al.*, Phys. Rev. Lett. **82**, 1391 (1999).
[3] C. Guénaut *et al.*, Phys. Rev. C **75**, 044303 (2007).
[4] A. Gade *et al.*, Phys. Rev. C **81**, 051304(R) (2010).
[5] S. Zhu *et al.*, Phys. Rev. C **85**, 034336 (2012).
[6] O. Sorlin *et al.*, Phys. Rev. Lett. **88**, 092501 (2002).
[7] K. Langanke, J. Terasaki, F. Nowacki, D. J. Dean, and W. Nazarewicz, Phys. Rev. C **67**, 044314 (2003).
[8] L. Gaudefroy *et al.*, Phys. Rev. C **80**, 064313 (2009).
[9] H. Nakada, Phys. Rev. C **81**, 051302(R) (2010).
[10] P. Adrich *et al.*, Phys. Rev. C **77**, 054306 (2008).
[11] F. Recchia *et al.*, Phys. Rev. C **85**, 064305 (2012).
[12] S. Suchyta *et al.*, Phys. Rev. C **89**, 021301(R) (2014).
[13] Y. Tsunoda *et al.*, Phys. Rev. C **89**, 031301(R) (2014).
[14] M. P. Carpenter, R. V. F. Janssens, and S. Zhu, Phys. Rev. C **87**, 041305 (2013).
[15] S. N. Liddick *et al.*, Phys. Rev. C **84**, 061305(R) (2011).
[16] D. Pauwels *et al.*, Phys. Rev. C **78**, 041307(R) (2008).
[17] S. N. Liddick *et al.*, Phys. Rev. C **85**, 014328 (2012).
[18] D. Pauwels *et al.*, Phys. Rev. C **79**, 044309 (2009).
[19] C. J. Chiara *et al.*, Phys. Rev. C **85**, 024309 (2012).
[20] T. Ishii, M. Asai, A. Makishima, I. Hossain, M. Ogawa, J. Hasegawa, M. Matsuda, and S. Ichikawa, Phys. Rev. Lett. **84**, 39 (2000).
[21] A. M. Oros-Peusquens and P. F. Mantica, Nucl. Phys. **A669**, 81 (2000).
[22] S. N. Liddick *et al.*, Phys. Rev. C (submitted).
[23] M. Pfützner *et al.*, Nucl. Phys. **A626**, 259c (1997).
[24] R. Grzywacz *et al.*, Phys. Rev. Lett. **81**, 766 (1998).
[25] M. Lewitowicz *et al.*, Nucl. Phys. **A654**, 687c (1999).
[26] M. Sawicka *et al.*, Phys. Rev. C **68**, 044304 (2003).
[27] H. Grawe *et al.*, Nucl. Phys. **A704**, 211c (2002).
[28] C. Mazzocchi *et al.*, Phys. Lett. **B622**, 45 (2005).
[29] C. J. Chiara *et al.*, Phys. Rev. C **84**, 037304 (2011).
[30] C. J. Chiara *et al.*, Phys. Rev. C **86**, 041304(R) (2012).
[31] F. Recchia *et al.*, Phys. Rev. C **88**, 041302(R) (2013).
[32] R. Broda *et al.*, Phys. Rev. C **86**, 064312 (2012).
[33] Noritaka Shimizu, Takashi Abe, Yusuke Tsunoda, Yu-

taka Utsuno, Tooru Yoshida, Takahiro Mizusaki, Michio Honma, and Takaharu Otsuka, Prog. Theor. Exp. Phys. **2012**, 01A205 (2012).

[34] T. Otsuka, M. Honma, T. Mizusaki, N. Shimizu, and Y. Utsuno, Prog. Part. Nucl. Phys. **47**, 319 (2001).

[35] W. F. Mueller *et al.*, Phys. Rev. C **61**, 054308 (2000).

[36] B. A. Brown (private communication).

[37] I. Y. Lee, Nucl. Phys. **A520**, 641c (1990).

[38] D. C. Radford, Nucl. Instrum. Methods Phys. Res. A **361**, 297 (1995); *ibid.*, 306.

[39] D. Bazin, J. A. Caggiano, B. M. Sherrill, J. Yurkon, and A. Zeller, Nucl. Instrum. Methods Phys. Res. B **204**, 629 (2003).

[40] I. Y. Lee *et al.*, Nucl. Phys. **A746**, 255c (2004).

[41] S. Paschalis *et al.*, Nucl. Instrum. Methods Phys. Res. A **709**, 44 (2013).

[42] I. Stefanescu *et al.*, Phys. Rev. C **79**, 034319 (2009).

[43] O. Perru *et al.*, Phys. Rev. Lett. **96**, 232501 (2006).

[44] M. M. Rajabali, Ph.D. thesis, University of Tennessee, 2009 [http://trace.tennessee.edu/utk_graddiss/648].

[45] M. M. Rajabali *et al.*, J. Phys. G: Nucl. Part. Phys. **41**, 115104 (2014).

[46] F. Flavigny *et al.*, Phys. Rev. C (submitted).

[47] E. Caurier, shell-model code ANTOINE, IRES, Strasbourg 1989-2004; Etienne Caurier and Frederic Nowacki, Acta Phys. Pol. B **30**, 705 (1999).

[48] NuShellX@MSU, B. A. Brown, W. D. M. Rae, E. McDonald, and M. Horoi, http://www.nscl.msu.edu/∼brown/resources/resources.html; NuShellX, W. D. M. Rae, http://www.garsington.eclipse.co.uk/.

[49] See endnote [28] in B. Cheal *et al.*, Phys. Rev. Lett. **104**, 252502 (2010).

[50] A. F. Lisetskiy, B. A. Brown, M. Horoi, and H. Grawe, Phys. Rev. C **70**, 044314 (2004).

[51] M. Honma, T. Otsuka, T. Mizusaki, and M. Hjorth-Jensen, Phys. Rev. C **80**, 064323 (2009).

[52] Coral M. Baglin, Nucl. Data Sheets **113**, 2187 (2012); Evaluated Nuclear Structure Data File (ENSDF), http://www.nndc.bnl.gov/ensdf.

[53] T. Otsuka *et al.*, Phys. Rev. Lett. **95**, 232502 (2005).

[54] Kris Heyde and John L. Wood, Rev. Mod. Phys. **83**, 1467 (2011).